· Article ·
doi: 10.13679/j.advps.2014.4.00269

Advances in Polar Science
December 2014 Vol. 25 No. 4: 269-282

An ice-ocean model study to explore climate change mechanisms in comparison with interannual-to-decadal variability of geochemical tracers

Motoyoshi Ikeda*

Hokkaido University, Kawasaki 213-0033, Japan

Received 17 February 2013; accepted 19 June 2014

Abstract One way to identify the mechanisms that are crucial to Arctic climate change is to use existing data that exhibit interannual-to-decadal variability in the sea ice and ocean interior due to atmospheric forcing. Since around 1960s, valuable geochemical data of the ocean interior, together with atmospheric and sea ice data, have been analyzed and examined in a coupled ice–ocean model with an idealized configuration of the Arctic Basin. This is fundamentally driven by negative salt flux, in addition to atmospheric circulation and cooling. This strategy has a clear advantage over more sophisticated models with higher resolution that require extensive data collections for verification. Around 1990, the dominant atmospheric mode shifted from the Northern Annular Mode (NAM) to the Arctic Dipole Mode (ADM). The variability of sea ice cover was explained by these two modes sequentially and reproduced in the model. In particular, the geochemical fields indicated a movement of the Transpolar Drift Stream due to the NAM and an oscillation of the Pacific water between the Atlantic and Pacific sides due to the ADM. Both these features were reproduced reasonably well by the oceanic tracers in the model, including the time lags of about one third of the oscillation periods. Thus, this strategy can suggest methods and locations for monitoring oceanographic responses to Arctic climate change.

Keywords **Arctic Ocean, ocean interior variability, geochemical data, model verification**

Citation: Ikeda M. An ice-ocean model study to explore climate change mechanisms in comparison with interannual-to-decadal variability of geochemical tracers. Adv Polar Sci, 2014, 25:269-282, doi: 10.13679/j.advps.2014.4.00269

1 Introduction

The most remarkable change observed in Arctic sea ice cover is the trend of reduction in its extent since 1970s, as shown in Figure 1. This trend is qualitatively consistent with the warming atmosphere, but it requires a quantitative explanation[1]. Based on the IPCC report (AR4), the summer ice cover is predicted to become minimal by the second half of the 21st century; however, the decrease in ice appears to be occurring at a rate faster than predicted[2]. In particular, the observed summer ice cover has already reached a record low: once in 2007 and then again in 2012. Therefore, its disappearance by 2020 appears plausible based on simple extrapolation with consideration of the basic concept of ice–albedo feedback. However, significant year-to-year variability might indicate that the prediction of such an early disappearance could be an exaggeration. The median of realistic coupled models was shown to reduce the Arctic sea ice cover to nearly an ice-free state by 2035[3]. Hence, it is important that we advance the understanding of the responses of the ice–ocean system to atmospheric variability.

The ultimate goal of climate research is to make reliable projections of future conditions using a global coupled atmosphere–ocean–cryosphere model[4]; however, this is not a simple task[5]. Among the many difficult challenges, improvements in the understanding of both the polar warming amplification and the ocean interior response are important

* Corresponding author (email: mikeda@ees.hokudai.ac.jp)

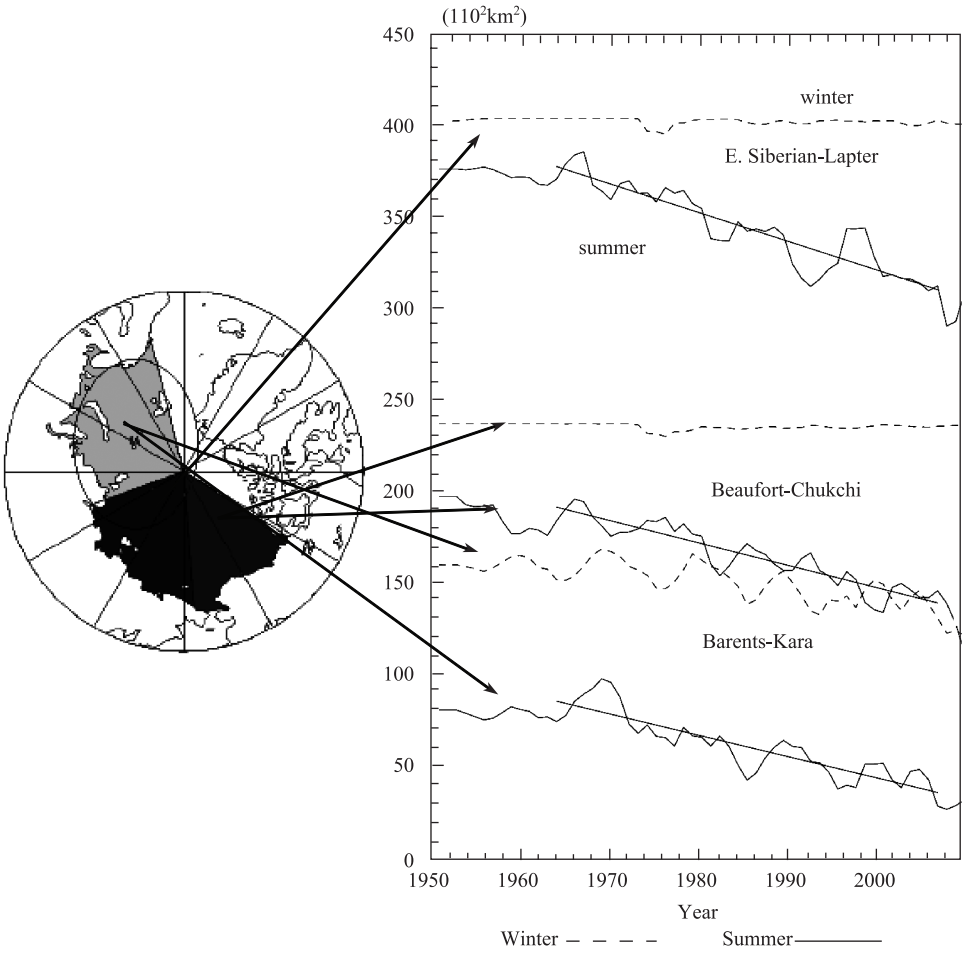

Figure 1 Ice cover trends and variations in three regions: the Beaufort–Chukchi Sea, East Siberian–Laptev Sea, and the Barents–Kara Sea, for winter (Dec–Feb) and summer (Jun–Aug). The ice cover time series were smoothed using a 3-year Hanning filter applied to the original data.

aspects of model development strategy, for which the interannual variability might provide critical and useful test cases. Polar amplification could be examined with a regional Arctic model nested within a global model, which is restored towards reanalysis fields. The ocean interior responses could be investigated using a coupled ice–ocean model forced with atmospheric reanalysis fields. With such an approach, verification data from the ocean interior are necessary; however, such data are very limited and should be treated carefully.

With regard to atmospheric variability and sea ice cover anomalies, the dominant modes have been fully described together with correlations between the atmosphere and sea ice[6]. The Polar Vortex is a major feature that has significant decadal oscillations, which was first reported as the Arctic Oscillation[7], but is now called the Northern Annular Mode (NAM). This mode contains fluctuations between stronger and weaker phases of the Polar Vortex, which are defined as the positive and negative NAM, respectively. Thus, the atmospheric circulation near the sea level is represented by weaker and stronger phases of the Beaufort High over the Canada Basin.

It has been suggested that the shift in the dominant atmospheric mode from the NAM to the Arctic Dipole Mode (ADM) with a positive pole located over Greenland and a negative pole over Siberia, occurred in the 1980s[6]. We attempt to investigate the role of the ocean general circulation, the response of which could take a few years to manifest. Hence, a smoothed time series is most appropriate for such a statistical analysis, and the low-pass filtered winter ADM was retrieved to determine the responses of sea ice and ocean circulation.

The coverage of sea ice in the Beaufort–Chukchi Sea, East Siberian–Laptev Sea, and Barents–Kara Sea is plotted in Figure 1. A three-year Hanning filter was used to produce the low-pass filtered ice coverage. Note that Ikeda[6] has previously described the full detail of the sea ice data, atmospheric data, and analysis methods. The minima in the East Siberian–Laptev Sea, and then in the Barents–Kara Sea two years later, matched the positive phases of the NAM (Table 1). In the Beaufort–Chukchi Sea, the ice cover increased two years after the NAM peaks. The contrasting variations between the Beaufort–Chukchi Sea and Barents–Kara Sea are reasonable based on the pattern of the NAM,

which weakens the Beaufort Gyre during its positive phase. If the NAM has a decadal oscillation, the anomaly of sea ice cover might behave as a perturbation propagating from the Beaufort–Chukchi Sea to the Barents–Kara Sea after about four years.

Table 1 Correlations between atmospheric variability and summer ice cover variability

	BC	EL	BK	BK−BC
NAM	0.04/0.36(2)	-0.29	-0.20/-0.26(2)	−
ADM	-0.37/-0.41(1)	0.18	0.14	0.38/0.48(1)

Note: BC, EL, and BK denote the Beaufort–Chukchi, East Siberian–Laptev and Barents–Kara seas, respectively. BK−BC denotes the ice-covered area in the Barents–Kara Sea minus that in the Beaufort–Chukchi Sea. Correlation coefficients are shown for simultaneous cases (i.e., 0-year lag) as well as for the highest correlations among the lagged cases between 3-year and -1-year lags, if they are higher than the simultaneous ones. Here, lags in parentheses represent the years by which the ice cover lags the atmosphere. Bold letters show significant correlations at a 95% confidence level, where the numbers of degrees of freedom are 20 under the consideration of the zero-correlation time scales in the auto-correlations.

The correlation coefficients with the winter ADM were calculated using the Hanning filter and trend removal for ice cover lagged by minus 1 to 3 a relative to the ADM. In Table 1, the coefficients with maximum magnitudes are listed, in addition to those with no lag, such that the time lag can be tested for significance. It can be seen that significant positive correlations were found (0.38 and 0.48 for 0- and 1-year lags, respectively), i.e., the ice cover decreased (increased) over the Beaufort–Chukchi Sea (Barents–Kara Sea) both in summers of the same year and one year after the positive winter ADM.

As there is much less coverage of observed data for the ocean interior than for sea ice, verification of numerical models has been limited. In a pioneering work of Arctic Ocean modeling[8], a coupled ice–ocean model simulated ice cover oscillations in response to the NAM reasonably well. The model also showed that the ocean circulation in the Arctic Basin swings between the Eurasian and Canadian sides; a feature for which we need data from the ocean interior for verification. Observed ice velocity fields were shown to vary in response to the NAM[9], i.e., the ice stream on the Transpolar Drift Stream shifted towards the Canadian and Eurasian sides during the positive and negative phases, respectively. Using properties of seawater observed at the North Pole, it has been proposed that the Arctic Basin responds to the NAM with a time lag of several years[10]. Therefore, ocean general circulation might not have played a major role in the processes associated with the single event in the summer of 2007[11]. By employing a high-resolution ice–ocean model to examine oceanic responses to the NAM[12], it was claimed that the Eurasian shelves send freshwater to the Lomonosov Ridge and Alpha–Mendeleyev Ridge during negative and positive NAM phases, respectively. Thus, the necessity of implementing an Arctic observing system to constrain the coupled ice–ocean models was highlighted[13].

Arctic Basin circulation is driven by the buoyancy flux associated with river discharge and low-salinity water from the Pacific[14], and exchanges of sea water with the North Atlantic. Therefore, the role of the deep ocean in ice cover anomalies due to the NAM and ADM should be investigated. A highly idealized ocean model could provide a basis for the density-driven Arctic Ocean, which could be coupled with a sea ice model[15]. The essential mechanism is a response of the basin-scale Arctic Ocean circulation to variable wind fields. Thus, the approach taken in the present study is completely different to high-resolution modeling[12].

The Russian hydrochemical data set collected from the Arctic Basin provides useful information regarding ocean interior variability over several decades[16]. Among the various chemical components, silicate identifies the boundary between the silicate-rich Pacific water and the contrasting Atlantic water. The boundary between the two water masses at around 200-m depth in the Canada Basin indicates the vertical motion of the Atlantic water on a decadal time scale: i.e., the boundary shifts upwards (downwards), as realized by silicate reduction (increase) at a fixed depth, responding to the more intense (weaker) Polar Vortex or the positive (negative) NAM. This valuable hydrochemical data set should be analyzed further for verification of Arctic Ocean models with interannual to decadal responses to atmospheric variability.

In section 2, the geochemical tracers of the Russian data set are analyzed and related to atmospheric variability. A coupled ice–ocean model is introduced in section 3, and model experiments with forcings from the NAM and ADM, which provide the responses of the sea ice cover and tracers in the ocean interior, are presented in section 4. Comparisons between the observed sea ice and geochemical fields and the model results suggest ways of verifying climate models and monitoring interannual-to-decadal variability produced by the dominant atmospheric modes. These outcomes together with conclusions are discussed in section 5.

2 Geochemical variability in the ocean

The mean states of dissolved oxygen have been described for the Arctic Basin[17], whereas interannual variability has not been examined in relation to atmospheric circulation variability. Various types of data have been collected both from the water and above the sea surface of the Arctic Ocean at drifting stations (North Pole Stations) by observers of the former Soviet Union observers. In addition to meteorological data, marine hydrochemical data have been considered to provide useful information regarding the Arctic[18], but few scientists have used them. As surface data force us to speculate with regard to the ocean interior, this relatively new data set from the ocean interior provides useful information on oceanic responses to atmospheric variability.

The geochemical parameters might represent biogeochemical processes and could perform as tracers

for identifying physical processes in the ocean. Chemical oceanographers will often use conserved values of geochemical parameters, e.g., a source region of the Halocline Water was identified by distinguishing the Pacific Water and the water mass influenced by the continental shelf[19]. In the present study, we attempted to determine ocean interior responses to atmospheric forcing on scales of several years to decades by tracing robust geochemical components, silicate, and dissolved oxygen.

Before describing the data analysis in the present paper, the reader is referred to Ikeda et al.[16] to appreciate the information common to the two studies. The hydrochemical data were used to explore oceanic variability as a response to atmospheric variability. The silicate data were distributed in the Arctic Ocean with high spatial heterogeneity. First, the spatial distribution of the mean state was constructed, and then a temporal deviation from the mean state was derived. Here, a layer below the surface mixed-layer was selected for the mean state construction without seasonal cycles, while the interannual-to-decadal variability was retained as temporal deviations. As shown in Figure 2, the mean silicate concentration is low in the Atlantic and increases into the Canada Basin with a distinct boundary around the Transpolar Drift Stream. In the vertical section, the Pacific Water contains much higher concentration (40 μmol·kg^{-1}) than the Atlantic Water (5 μmol·kg^{-1}).

Ikeda et al.[16] focused their analysis on the vertical motion in the Canada Basin. The Pacific Water inflow, with moderate biological effects, was considered to create a clear maximum concentration between 100 and 200 m in the Canada Basin. The values at 200-m depth provided a robust signal of vertical water motion extracted from the boundary between the Pacific water and the Atlantic water. The negative correlation between the silicate anomaly and the NAM, which represented an upward shift in the water column, suggested that less silicate occurred under conditions of a more intense Polar Vortex or positive NAM. A more intense Polar Vortex induced an outward Ekman flux in the Canada Basin and hence, Ekman divergence led to an upward motion in the upper ocean. The time lag was less than or equal to 1 a, implying a nearly instantaneous response within one year. Using the same model as that introduced in section 3, a preliminary test was made to illustrate that the upper ocean shifted vertically in the Canada Basin in response to the NAM[20].

Following the successful analysis of the vertical motion, horizontal oceanic motion was investigated in the present study using geochemical data averaged over a rectangular domain around the Transpolar Drift Stream. The peak of silicate at 100-m depth (Figure 2a) was used to detect the horizontal motion between the Pacific and Atlantic sides. Dissolved oxygen exhibited a horizontal distribution contrasting that of silicate, in addition to higher values near the sea surface due to the atmospheric exchange (Figure 2b), i.e., it was higher on the Atlantic side (8 mL·kg^{-1}) than the Pacific side (5 mL·kg^{-1}). Both silicate and oxygen data

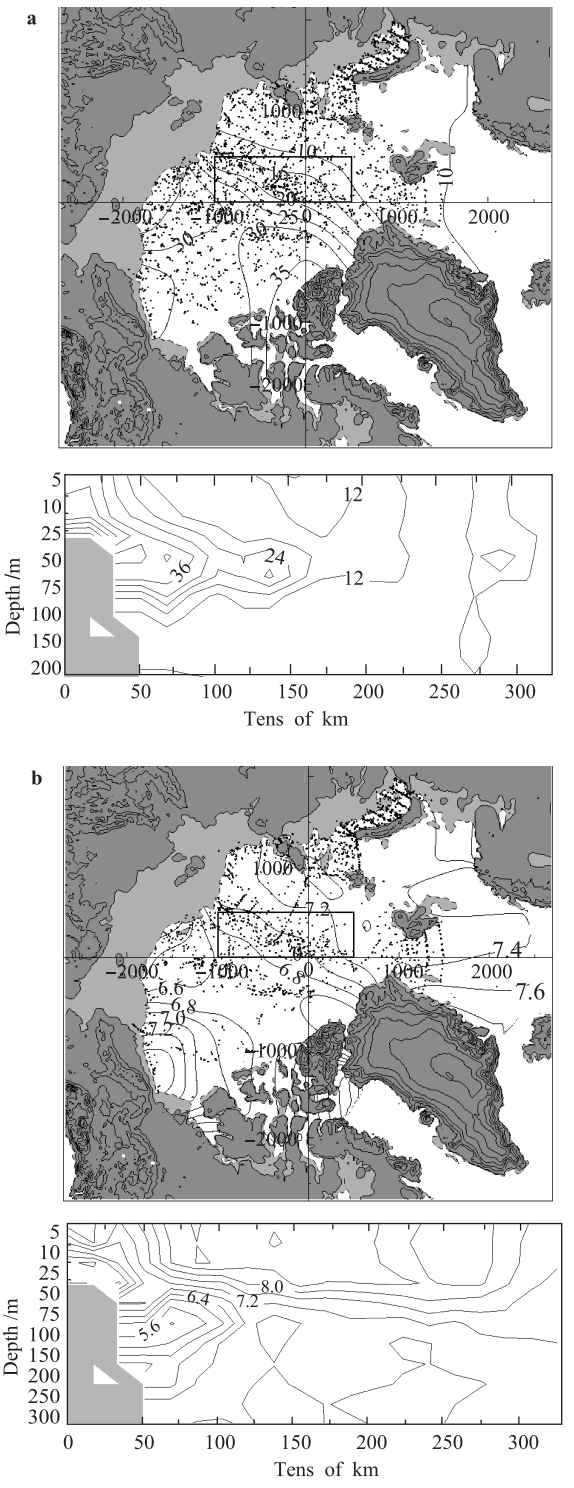

Figure 2 Plan views of silicate (**a**) and dissolved oxygen (**b**) at 100-m depth, and the cross section from the Pacific sector (180°) to the Atlantic sector (0°). Dots denote the locations of data collection, and the units are μmol·kg^{-1} (**a**) and mL·kg^{-1} (**b**). The rectangular domain is the region over which silicate was averaged around the Transpolar Drift Stream.

from 100-m depth were processed and plotted in Figure 3 to determine their annual means, together with the NAM and

ADM time series. The silicate data were limited to the period 1965–1985, while the dissolved oxygen data encompassed 1965–1995. The correlation between them is most significant for silicate lagged from dissolved oxygen by 2 a (Table 2).

Table 2 Correlations among two ocean interior parameters (silicate and oxygen), the atmospheric parameters (NAM and ADM), and sea ice cover difference (the Barents–Kara Sea minus the Beaufort–Chukchi Sea)

	Period	0-year	Max
Silicate/oxygen	1967–1984	-0.20	-0.50 (2)
Silicate/NAM	1967–1984	0.55	-0.82 (4)
Oxygen/NAM	1967–1996	-0.25	0.68 (3)
Oxygen/ADM	1967–1996	-0.08	-0.55 (2)
Oxygen/ADM	1976–1996	-0.17	-0.67 (2)
Oxygen/ice summer	1967–1996	-0.35	-0.66 (2)
Oxygen/ice summer	1976–1996	-0.49	-0.75 (1)

Note: The time series were smoothed using a 3-year Hanning filter and their trends removed. 'summer' denotes the season in which the ice cover was measured. 1967–1984', '1967–1996' and '1976–1996' denote the periods of 1967–1984, 1967–1996, and 1976–1996 for which the ADM and summer ice cover values were taken. Correlation coefficients are shown for simultaneous cases (i.e., 0-year lag) and maximum magnitudes. The values in parentheses denote the lags by year by which the former parameters (e.g., silicate) lag the latter parameters (e.g., NAM). Bold letters show significant correlations at a 95% confidence level, where the numbers of degrees of freedom are 10 for the 20-year period and 15 for the 30-year period.

Both silicate and dissolved oxygen were correlated with the NAM. As dissolved oxygen showed larger amplitude fluctuations before 1985, the main contribution to the correlation was made by the period 1965–1985. Low silicate and high oxygen exhibited correlation with the positive NAM at 4- and 3-year lags, respectively. The swing directions were similar to the model results[8], as with the shift of the Transpolar Drift Stream towards Canada and Siberia in response to the positive and negative phases of the NAM. However, it is noted that the geochemical fields indicated 3- to 4-year lags from the positive NAM in the present study. A more detailed characteristic of the responses was the longer duration of the silicate anomaly compared with that of oxygen, i.e., during the period from the positive to negative peaks of the NAM (1973–1978), oxygen returned to the decreasing phase in 1976 and silicate started increasing in 1977.

A correlation with the ADM was expected for dissolved oxygen, the data for which were collected after 1985. We focused on the period after 1976 for the correlation between the dissolved oxygen and the ADM (Table 2). Oxygen demonstrated a significant correlation with the ADM with a 2-year lag. This time lag is consistent with the lag of 1 year from the ADM to the summer ice difference between the Pacific and Atlantic sides, leading to a lag of one year from the summer ice difference to the oxygen. Thus, these time lags have actual geophysical meaning, even though the Hanning filter was applied to the time series. These correlations are also shown in Figure 3, particularly after 1985. A straightforward interpretation is that wind stress pushed sea ice from the Pacific to the Atlantic sector of the Arctic[6] and also drove ocean circulation, such that the geochemical features contained in the Pacific water shifted to the Atlantic side. In the following, the idealized numerical model is verified for the ADM using the hydrochemical fields.

3 Coupled ice–ocean model configuration

3.1 Ocean model

The ice–ocean model used in this study is based on an idealized ocean general circulation model developed by Ikeda[15]. It was used to examine the response of buoyancy-driven circulation to wind stress with the objective of clarifying the circulation in the region of Baffin Bay and the Labrador Sea. The original ocean model had two levels on a frictionless flat bottom in a rectangular basin, and it was forced by positive and negative buoyancy fluxes in the northern and southern portions, respectively. The zonal velocity was assumed to be in geostrophic balance with the meridional density gradient. The principal behavior of the model is as follows. The meridional overturning driven by the buoyancy fluxes is baroclinic with a southward (northward) flow in the upper (lower) level. The wind-driven circulation is mostly barotropic with the baroclinic component reduced by horizontal diffusion. The upper-level southward flow shifts to the western (eastern) boundary under cyclonic (anticyclonic) wind stress curl. With oscillatory wind stress curl, the southward buoyancy transport is intensified (weakened) while the curl switches from anticyclonic to cyclonic (cyclonic to anticyclonic). The adjustment period is about 100 d and is proportional to the domain area.

The original model was modified for use in the present study for application to the region of the Arctic Basin and Greenland Sea. It is also noted that the ocean model was highly idealized in comparison with the primitive equation model[21]. The ocean model had two levels: an upper-level thickness of 300 m and the rest of a water column with total depth varying from 1 500–4 000 m, except for the BarentsSea, which was 300 m (Figure 4a). The model domain was composed of four rectangular areas: the Canada Basin, Eurasian Basin, Barents Sea, and Greenland Sea. The bottom topography was also simplified to have straight contour lines in each area. The model only had a coarse horizontal resolution of 100 km×100 km for the offshore region of the continental shelves.

The upper level contained a bulk surface mixed-layer[22], which developed because of the kinetic and potential energy inputs through the ice–ocean interface and the sea surface in ice-free portions by following the turbulent closure scheme. The barotropic component was determined based on the conservation of volume and potential vorticity under rigid

lid conditions, in the same manner as the primitive equation model, whereas the baroclinic component was assumed in geostrophic balance. This baroclinic component imposed the constraint that a baroclinic Kelvin wave, which played only a minor role in the present case, was not allowed along the coastal boundaries.

3.2 Sea ice model

The ocean model was coupled with an ice model that is consistently used for the polar oceans[23-24], although it was simplified in terms of some configurations. The ice component was governed by the ice mass balance with advection, diffusion, and formation/melting, and by the momentum balance. Sea ice concentration A was not calculated separately from the ice mass, but related to ice volume per unit area V ($m^{-3}\cdot m^{-2}$) (i.e., $A = 1 - \exp(-2V)$). Thus, A was approximately 0.9 for 1-m-thick ice and it approached $2V$ for very sparse ice. This approximation was equivalent to a minimum ice thickness of 0.5 m, which was assumed for newly formed ice in the two-category ice model developed by Hibler[23]. Sea ice in the present study had no explicit consideration of ice ridging and rafting.

The momentum balance retained wind stress, ice-water stress, the Coriolis force, and gravity due to an ocean surface tilt, whereas internal ice stress was replaced with viscosity at a coefficient of $5\times10^{3}m^{2}\cdot s^{-1}$ in the quadratic form instead of the viscous-plastic model. The viscous model has weak resistance against convergence and thus, it might overestimate ice thickness, particularly near the Canadian coast. The model results were examined for this behavior in section 4.

Air–ice heat fluxes were calculated in the usual way, i.e., by considering shortwave and longwave radiation, and sensible and latent heat fluxes. The formulations and coefficients of thermodynamics were similar to those used in the series of ice–ocean modeling studies by Ikeda et al.[20] and Hiraike and Ikeda[24], both of which were based on original thermodynamic formulations by Ikeda[25]. Sea ice started to form once ocean temperature fell to freezing point, which was set at –2°C. Heat loss (gain) through the open water and

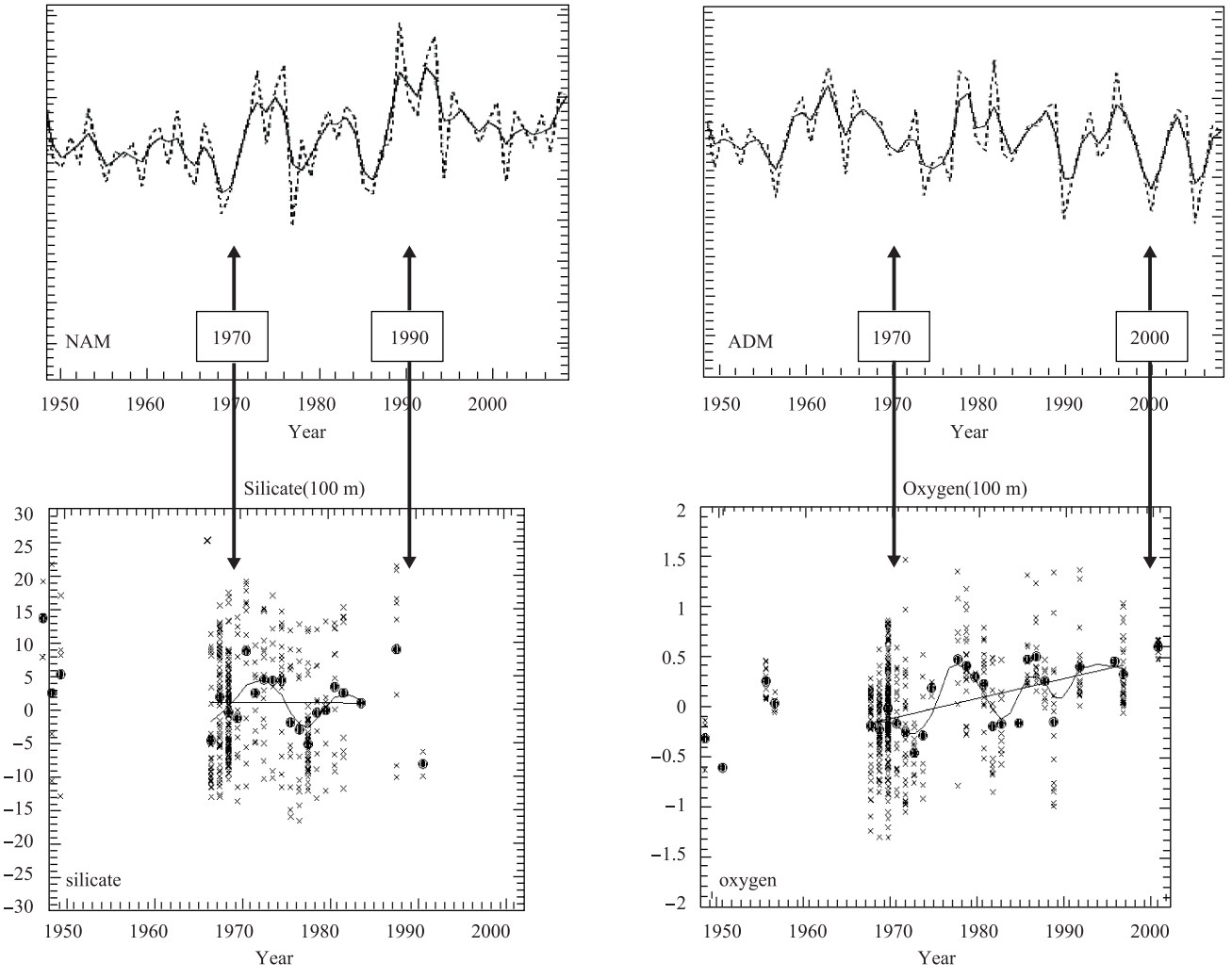

Figure 3 Individual data (cross) and annual mean anomalies (large circle) of silicate and dissolved oxygen over the rectangular domain in Figure 2, where a 3-year Hanning filter was applied on the original time series of the annual mean, together with linear interpolation for missing years. The NAM and ADM time series in winter are also taken from Figures 2 and 4, respectively, of a previous study[6].

ice was converted to an increase (a decrease) in ice volume. The ice volume in a unit area increased (decreased) when advection caused ice convergence (divergence).

3.3 Atmospheric and other forcing

In the present model, sea-level pressure (SLP) was specified, giving air–ice drag and air–water drag along the SLP contours; hence, sea ice was pushed along the wind direction. Therefore, the shear between the sea ice and water in the mixed layer was determined from an SLP gradient, having a coefficient of 1/(air density multiplied by the Coriolis coefficient). In the configuration fully described with atmospheric and ocean dynamics, a spiral of wind direction existed in the atmospheric boundary layer and an Ekman spiral maintained the shift in the mixed layer. However, the differences in ice motion were minor between the present model, full model, and actual state in free-drifting conditions, where the deviation angle between the geostrophic wind and surface wind was approximately balanced by the deviation angle between the surface wind and ice drift.

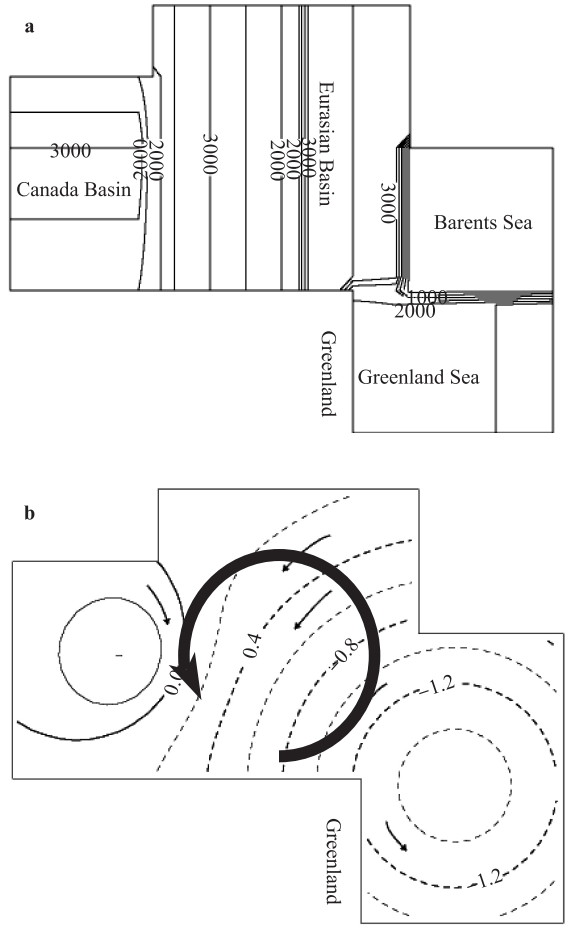

Figure 4 Coupled ice–ocean model geometry with bottom topography (unit in m (**a**)), and the mean sea level pressure field (**b**), together with a schematic view of the NAM circulation (bold arrow) and the mean wind directions (thin arrows). The unit is hPa.

In addition, the wind field was composed of the annual mean and synoptic field , i.e., the mean could be seasonal or monthly as long as the time scale of variability was much longer than the synoptic field. Wind stress was approximated to be proportional to the square of the wind speed. A typical synoptic field is a rotating vector with constant amplitude. Under the assumption that the synoptic field was dominant over the mean field, the mean wind stress was determined as being proportional to the mean wind velocity by taking the lowest order. The relationship in the present configuration produced ice–water shear of about 0.01 $m \cdot s^{-1}$ at the seasonal mean, which was consistent with the annual mean ice velocity in the Arctic Basin[25]. By combining these effects, the proposed formulation was verified against the observed field in section 4.

The SLP field was expressed with a cyclonic circulation over the entire Arctic Basin with a minor anticyclonic circulation over the Beaufort Sea (Figure 4b). The SLP structures were weak because the domain was only above 70°N. The time-dependent components represented interannual variability and were superimposed on the steady circulation, e.g., the NAM was given a rotation with its center and amplitude of –1 hPa at the North Pole. To imitate synoptic weather, an additional wind of 5 $m \cdot s^{-1}$ with a 5-day cycle was always given only to the development of the mixed-layer and air–ice and air–ocean heat fluxes, where the synoptic wind had a zero mean value.

The air temperature and shortwave radiation were given with sinusoidal annual cycles, i.e., the air temperature had a maximum of 0℃ and a minimum of –20℃ over the Arctic Basin (Canada and Eurasian basins), and the shortwave radiation was within the range 200–0 $W \cdot m^{-2}$. The annual cycles in air temperature were smaller in the other regions, as the minimum values were set at –5℃ over the Greenland Sea and –10℃ over the Barents Sea. Relative humidity was fixed at a constant value of 0.8. No interannual variability was given to air temperature or shortwave radiation, although the model could be tested with interannual variability.

Some portions of the ocean were restored to climatic conditions, i.e., temperature and salinity were restored to –2℃ and 33.0 in the upper level of the Canada Basin, while they were restored to –1℃ and 35.05 in the lower level. For the Greenland Sea, the restored values were 0℃ and 34.9, and –1.2℃ and 35.0 in the upper and lower levels, respectively. The e-folding time scales for restoration were 3 a and 300 a in the upper and lower levels of the Canada Basin, respectively and similarly, 1 a and 100 a for the Greenland Sea. The 3-year e-folding time scale allowed seasonal cycles in the upper level of the Canada Basin. It is noted that the surface mixed layer was not restored directly, whereas it received indirect restoration from the upper level below during mixed-layer development. This restoration provided a buoyancy-driven system with positive and negative buoyancy fluxes in the Canada Basin and Greenland Sea, respectively. This was confirmed not to ruin the responses in the Arctic Basin to the NAM and ADM, because major variability occurred in the

Eurasian Basin. For the purposes of tracking water masses, an artificial tracer was inserted in the upper level of the Canada Basin by restoration to a constant value.

4 Model results

4.1 Model verification for climatology with seasonal cycles

The period of the model run was 72 a towards an equilibrium state with a seasonal cycle. The final 1-year solution is examined here. The numerical solutions, shown in Figure 5, were verified against ice cover and ocean circulation determined by observed fields and other numerical models. As the upper level was restored to freezing point in the Canada Basin, it was natural to reproduce the permanent ice cover. Thus, the verification was concentrated on ice thickness, which increased towards the Canadian coast and exceeded 10 m. This value was a little higher than the thickness determined in the high-resolution model[26], showing the tendency towards viscous ice. The Barents Sea became ice free in summer. The general thickness distribution looked similar to the widely accepted values[27], whereas the Greenland coast had much less ice in the model, probably because no shelf region was included, and the restoring temperature was too high for ice formation in the Greenland Sea.

The Canada Basin was covered by an anticyclonic circulation in the upper level, together with a much weaker cyclonic circulation in the lower level. This feature is consistent with the observed flow pattern[28], which shows that the circulation in the Canada Basin was sensitive to the development of the under-ice mixed-layer and required careful selection for mixing parameterization. The upper level showed the Transpolar Drift Stream towards the Fram Strait at about 0.02 $m \cdot s^{-1}$, which can be mainly explained by baroclinic shear in relation to the horizontal density gradient (Figure 5c). The illustrated flow pattern was similar to the idealized case[15]. This suggests that a buoyancy-driven circulation is an essential mechanism for the baroclinic flow pattern in the Arctic Water layer, from the Canada Basin to the Eurasian Basin, above the reversal flow in the Atlantic Water layer. The ice–water shear was about 0.01 $m \cdot s^{-1}$, which was summed to a sea ice velocity of 0.03 $m \cdot s^{-1}$, in the same order of magnitude as the more realistic model[26]. Thus, the annual ice motion could be estimated to be 1 000 km along the Transpolar Drift Stream.

In the lower level (Figure 5d), a continuous current existed from the Greenland Sea to the Arctic Basin, flowing along the boundary between the Barents Sea and the Eurasian Basin, in a similar way to the model solution[28]. Another continuous current was revealed over the Lomonosov Ridge; however, the position was not clearly limited to either the northern or the southern side of the ridge, because of the coarse resolution of the model. The outflow was robust in the upper level from the Arctic Basin to the Greenland Sea and hence, mass conservation was supported by the inflow in the lower-level circulation. In summary, the model results were appropriate for the examination of oceanic responses to the NAM and ADM.

4.2 Responses to NAM

Following the 72-year simulation towards the equilibrium state, the model was run for three cycles of the NAM; which was observed to be nearly decadal and it was given a 12-year cycle in the present study. The NAM in the model had an SLP magnitude of 1 hPa without seasonal variability, centered at the North Pole. The NAM began at zero, initially became positive and then went through a negative phase, i.e., the SLP adopted negative and then positive anomalies. Unless indicated, the solutions are shown for the differences between the NAM case and the reference case, for which the 72-year simulation was extended for a further 36 a without SLP variability.

The solutions were taken from the third 12-year cycle and examined. The sea ice volume distributions, illustrated in Figure 6, show that the differences from the reference case are nearly symmetric between the positive (year 99) and negative (year 105) phases. The area of less ice appears to move from Canadian side to the Eurasian side, having a negative peak in the eastern part of the Eurasian side during the positive peak of the NAM (year 99). At the same time, the area of more ice starts on the Canadian side at year 99, shifts to the eastern part of the Eurasian side at year 105, and towards the western part at year 108. This progression is consistent with the observed one (Table 1). We might interpret the progression found both in Mysak and Venegas[29] and the present result as if the ice anomalies appeared on the Canadian side and propagated westwards to the European side in a clockwise direction across the Arctic Basin, although the real mechanism will be explored in the following section.

The ice anomaly was averaged in the Transpolar Drift Stream area and this is shown in Figure 7. The minimum appeared with a 1-year lag from the SLP minimum (positive NAM peak). The tracer, which had high concentration in the upper level of the Canada Basin, flowed out in the Transpolar Drift Stream and showed a negative peak with nearly a 4-year lag from the positive NAM peak. This feature is quite similar to that shown by silicate (Table 2). Thus, the Transpolar Drift Stream swung between the Canadian and Eurasian sides with a 4-year lag from the positive and negative NAM peaks, respectively. The Arctic Basin in the present model had a size of 2 000 km×3 000 km, which was 15 times larger than the size (400 km×1 000 km) in the idealized model[15], which showed an adjustment time of about 100 d. Hence, the adjustment time scale was estimated to be 1 500 d or about 4 a in the present case, which demonstrates that the model responses are quite consistent between the present model and the idealized one. The interpretation of the responses is that the mass transports between the regions of low and high density are modified by the wind-driven circulation. For example, the Transpolar Drift Stream between the Arctic

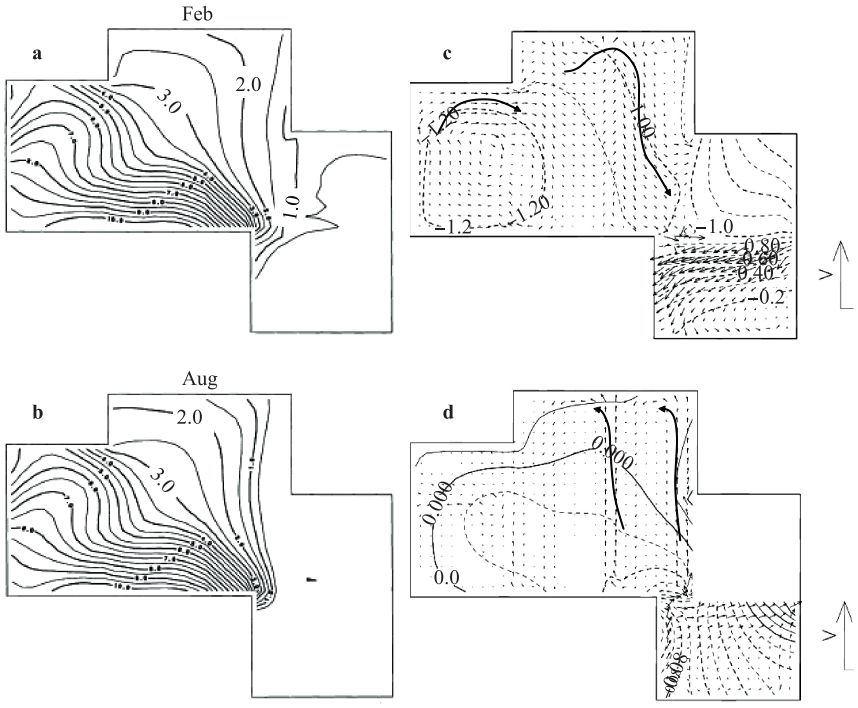

Figure 5 Sea ice volume per unit area V produced in the model for February (**a**) and August (**b**) with a contour interval of 0.5 m. As the volume becomes higher, concentration approaches unity in the model, such that the volume might be very close to thickness. Velocities and salinity relative to 35.0 in the upper level (**c**) and the lower level (**d**). The unit vectors represent 0.1 m·s^{-1} and the contour intervals are 0.1 (**c**) and 0.01 (**d**) . The solid and dotted lines denote positive and negative values, respectively.

Ocean and the Greenland Sea shifts to the Canadian (Eurasian) side because of the cyclonic (anticyclonic) circulation, which is driven by wind during the positive (negative) NAM.

The ice–ocean system showed responses that gradually changed with time from the first 12-year cycle to the third cycle of the NAM. The seasonal cycle of sea ice was intensified in the first cycle because of the larger atmospheric effects due to less sea ice, although the amount of sea ice accumulated as time proceeded. The tracer was more tightly stored in the Canada Basin without the NAM, and the swinging Transpolar Drift Stream showed a sharp gradient of the tracer in the first cycle. As the oscillation diffused the tracer, the 12-year fluctuation became smaller in the third cycle. The base tended to increase as time proceeded because the fluctuation extended the tracer under the conditions of the restoration in the Canada Basin; while these trends were not visible in the observed fields.

By considering the kinematic responses of the ice–ocean system to the NAM, sea ice was driven to the Canadian and Eurasian sides during the positive (year 99) and negative (year 105) NAM phases, respectively. Following this, the Transpolar Drift Stream shifted to the Canadian and Eurasian sides 4 a after the positive and negative peaks of the NAM, respectively. The Transpolar Drift Stream swung to the Canadian (Eurasian) side and pushed sea ice off (onto) the Barents–Kara Sea coast in year 103 (year 109). These two types of oscillation collaborated in producing the ice cover anomalies, which appeared to propagate from the Canadian, to the eastern Eurasian to western Eurasian sides before returning to Canadian side within the decadal oscillations (Figure 6); however, no mechanism exists for the propagation from the western Eurasian side to the Canadian side.

In the high-resolution ice–ocean model[12], freshwater flowed out of the Eurasian shelves in the western and eastern portions during the negative and positive NAM phases, respectively. In the present study, the continental shelves were not necessary to model the swing of the Transpolar Drift Stream. The fundamental behavior of the Transpolar Drift Stream was well explained by the responses of the buoyancy-driven general circulation to wind stress variability, as originally proposed by the idealized model[15]. This mechanism should also be investigated using a high-resolution model and thus, geochemical data might be useful for the verification of both the idealized and realistic ice–ocean models.

4.3 Responses to ADM

The ADM was given as variable SLP with one core over Siberia and another over Greenland with opposite signs, following the initial 72-year spin up. Both cores had amplitudes of 1 hPa and Gaussian distributions with e-folding radii of 1 500 km. The oscillation occurred with a 6-year cycle. The SLP over Siberia started with zero, turned

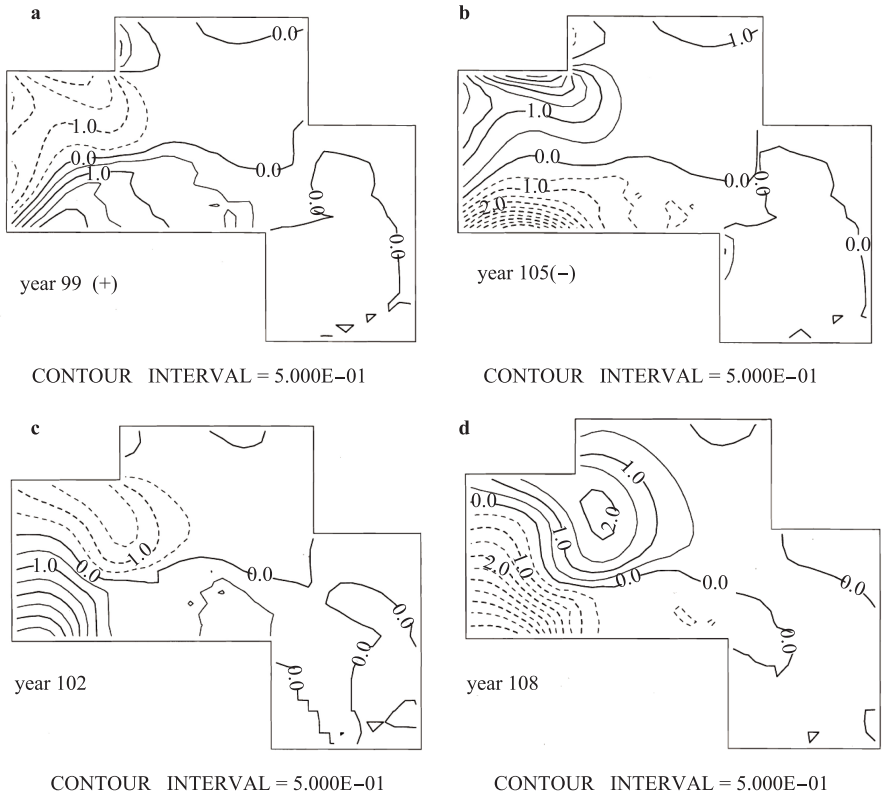

Figure 6 Difference in the sea ice volume per unit area V between the NAM case and the reference case in February for year 99 (NAM positive), 102, 105 (NAM negative), and 108. The contour interval is 0.5 m. The solid and dotted lines are for positive and negative values, respectively.

negative, and then changed to positive, i.e., the ADM initially became positive and then reversed. Within this 6-year cycle, sea ice was pushed to the Atlantic sector during the first half and then to the Pacific sector.

Once the ADM caused the sea ice to flow towards the Atlantic sector, the ice volume increased in the Barents–Kara Sea with a 1-year lag from the peak of the positive ADM (Figure 8); i.e., the Beaufort–Chukchi Sea showed an inverse progression (figure not shown). In the observed fields, the progression was revealed clearly only in the Beaufort–Chukchi Sea (Table 1). The seasonal cycle was enhanced by the ADM for the same reasons as for the NAM. This time scale was much shorter than that for the sea ice to move from the Pacific side to the Atlantic side, which was estimated to be 3 a (distance of 3 000 km divided by velocity of 1 000 km per year), suggesting the importance of convergence against and divergence from the corresponding coast lines.

A high peak of the tracer appeared with about a 3-year lag in the Barents–Kara Sea, indicating that the response of seawater was longer than that of sea ice. The response shown in oxygen was consistent with the model tracer (Table 2), where we should note that the sign is opposite. Wind anomalies produced Ekman divergence and convergence on the Eurasian and Canadian sides, respectively; however, Sverdrup circulation did not propagate westward because of very weak planetary β-effects. Under an oscillatory atmospheric forcing, an ocean circulation anomaly reached a peak with a lag from the atmosphere by a quarter of the oscillation period. Then, the ocean circulation anomaly returned to zero after a further quarter of the oscillation period. This is the reason why the trans-Arctic Ocean current continued to carry the tracer from the Pacific to the Atlantic sides for three years after the ADM peak. Therefore, the peak of the tracer that is high in the Canada Basin appeared in the Barents–Kara Sea for a half cycle, after the wind forcing reached a maximum strength pushing the tracer towards the Barents–Kara Sea. In addition to the oscillatory variations, the base increased after the ADM began, indicating that the Barents Sea contained more water of Pacific origin as long as the ADM persisted. Thus, wind variability tended to mix seawater horizontally in the Arctic Basin in response to both the NAM and the ADM.

5 Discussion and conclusion

The results are summarized in Figure 9 with reference to the case for sea ice[6]. SLP fields were dominated by the winter ones, and possessed the NAM as the first EOF and the ADM as the second EOF. The dominant atmospheric mode shifted from the NAM to the ADM around 1990. The low-pass filtered variability of sea ice cover was explained by these two modes sequentially, i.e., the decadal ice cover variability

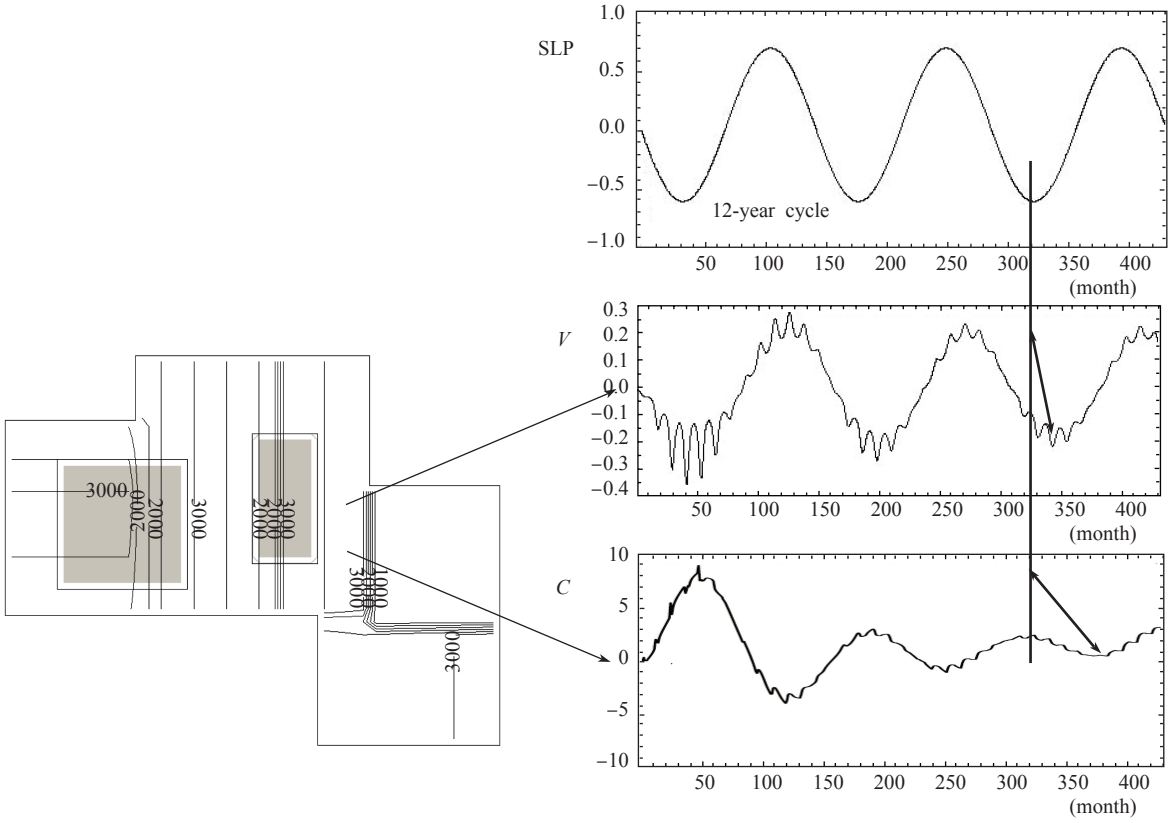

Figure 7 Differences between the NAM case and the reference case in SLP (unit in hPa) at the North Pole. The shaded areas denote the Transpolar Drift Stream and Canada Basin. In the Transpolar Drift Stream, sea ice volume per unit area V (unit in m) and the artificial tracer C in the upper level are plotted with the horizontal axes of months. The tracer is restored to 100 in the upper level of the Canada Basin and to 0 in the Greenland Sea and in the lower level everywhere.

was significantly correlated with the NAM until 1990 (Table 1, Figure 7). After 1980, the positive ADM with a low anomaly over Siberia and a high anomaly over Greenland induced low (high) ice cover in the Pacific (Atlantic) sector in one year (Figure 8).

As presented with the coupled ice–ocean model and the geochemical data, the ADM produced the ocean general circulation and caused the Pacific water to spread towards the Atlantic side in 2 a (Figure 8). The positive NAM also induced the ocean interior variability with the Transpolar Drift Stream shifting towards the Canadian side within 3 a or 4 a (Figure 7). The effects on sea ice cover matched with the peaks of the NAM over the East Siberian–Laptev Sea as a low anomaly, and showed within 2 a as asymmetric anomalies between the low in the Barents–Kara Sea and the high in the Beaufort–Chukchi Sea (Figure 6).

An interesting and useful finding of the present study is an effective mixing mechanism in the Arctic Ocean due to oscillatory motions, i.e., the ADM enhances horizontal mixing and modifies water structures more effectively than the NAM (Figures 7 and 8). The mixing yields the spread of the Atlantic Water into the Canada Basin and its consequent warming, and the outflow of the Pacific Water from the Canada Basin to the Atlantic side. It is reasonable to expect that the ADM might be more effective for sea ice reduction than the NAM. It is noted that the present model was forced with the restoration of the tracer in the Canada Basin, whereas actual tracers could be maintained by different mechanisms. The mixing effect is at a higher order than the original oscillations and therefore, it is difficult to verify with the geochemical fields.

The model variability was induced by SLP only, while air temperature also varied in the data[7]. An additional experiment was performed with sinusoidal air temperature higher (lower) by 1˚C when the SLP was lower (higher) by 1 hPa, by considering only the order of magnitudes from the reanalysis fields (not shown). This case amplified the ice cover variability by about 50%. Thus, the results in this study captured the essential features of the ice cover variability responding to atmospheric variability, while the actual sea ice anomalies might be enhanced in the data.

No shelf was implemented in the present model, although the shelf was found to play an important role in the high-resolution model[12]. Based on the present study, we could suggest that the general circulation in the Arctic Basin might have a major effect on the ice cover anomalies and on variations in the shelf circulation. Further modeling work is required to identify interactions between the shelf circulation and the basin-scale circulation.

The present study compared the results of an idealized ocean model with the geochemical data collected from

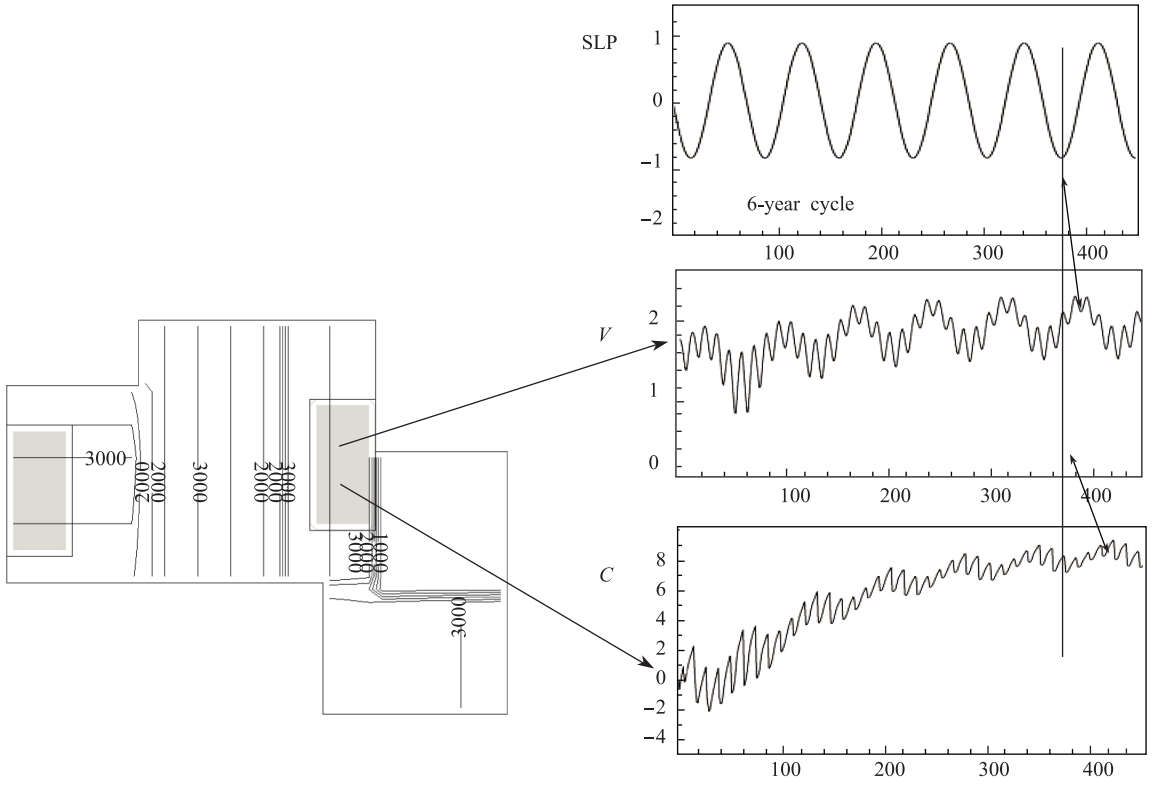

Figure 8 SLP (unit in hPa) over Siberia, sea ice volume per unit area V (unit in m), and the artificial tracer C in the upper level of the Barents–Kara Sea with the horizontal axes of months. V itself in the ADM case is shown, while SLP and C are the differences between the ADM case and the reference case. The box near the Pacific sector was used to analyze sea ice cover in the Beaufort–Chukchi Sea.

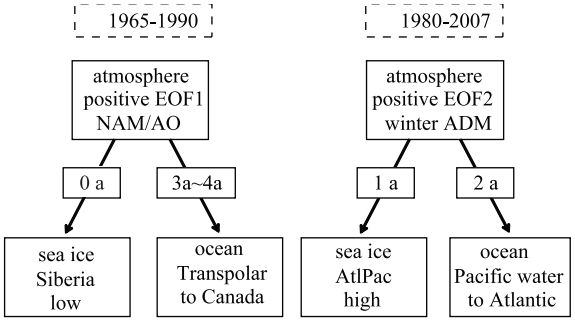

Figure 9 Summary of relationships among the atmospheric modes, sea ice cover, and ocean interior. Transition in the most influential atmospheric mode is suggested from NAM to ADM during the 1980s. The sea ice features are specified to be low ice cover over the East Siberian–Laptev Sea and the ice cover difference (Atlantic sector minus Pacific sector) for the earlier and later periods, respectively. The ocean interior responses are the swing of the Transpolar Drift Stream to the Canadian side and the movement of the Pacific water towards the Atlantic for the earlier and later periods, respectively. The time lags are presented for the lags from the atmospheric modes, positive NAM, and ADM.

drifting stations in the Arctic Ocean. This attempt could be extended to more realistic ocean models with high resolution. Model verification is a necessary step towards climate change prediction using high-resolution models, and various important mechanisms have to be reproduced in the models, e.g., sea ice ridging, ice band formation, inertial oscillation, double diffusion, step-like stratification, wind-waves in polynyas, and shelf waves.

Another direction would be a field study with the clear aim of exploring interannual variability in the Arctic Ocean. Based on the findings of the present study, two important areas can be identified: one is the position of the Transpolar Drift Stream, and the other is the contrast between the Pacific sector and the Atlantic sector. We should remind ourselves that dissolved oxygen and nutrients reflect biological production and its decomposition[30], and hence additional components have to be measured to separate related biological mechanisms from the water movement. This analytical idea becomes more crucial for processes with longer time scales such as global warming. Once the fine vertical structures of geochemical components are observed, interleaving of shelf water into the Arctic Ocean could be verified more closely[17]. This is an example of the challenges to be addressed by high-

resolution modeling and dedicated geochemical monitoring.

A number of authors have used coupled ice–ocean models for simulating the signals in the Arctic seas, which have been verified by comparison with data. The models duplicate well the ice cover variability in the Arctic Ocean, Labrador Sea, and Okhotsk Sea for seasonal cycles and decadal variability, whereas the oceanic responses have not been properly compared. Both modeling and observational approaches should be coordinated such that tools that are more reliable could be provided for predicting future changes in the Arctic seas. The NAM and ADM will not necessarily follow the past statistics under conditions of extremely low ice in the Arctic Ocean. An ultimate attempt would be to use a coupled ice–ocean–atmosphere model, in which crucial mechanisms should be tackled to enable us to derive answers for the questions that might arise when the Arctic sea ice becomes seasonal ice cover.

In the present study, only responses in the upper layer were investigated as indicators of decadal-to-interannual variability. As the time scales increase to multi-decades, we should be concerned with the lower layer below 2 000-m depth over the region from the Canada Basin to the Greenland Sea. The possibility of reactions occurring in the lower layer was proposed as an important mechanism for sea ice cover and upper layer structure under conditions of climate change[31]. This aspect should be examined closely with regard to a monitoring plan and model verification of the Arctic Ocean.

It is well accepted that wind stress provides dynamical effects more directly to sea ice and the ocean than atmospheric pressure does. A new approach was proposed by Wu et al.[32] based on complex vector empirical orthogonal function analysis. As this method is capable of resolving a pattern that shifts in space, we could apply such an innovative method to describe how propagating wind patterns contribute to the variability of sea ice extent. Some common findings were achieved between their analysis and Ikeda[6], e.g., the ADM is very effective with regard to anomalies of sea ice extent in summer over the East Siberian–Laptev Sea.

In addition to the effects of atmospheric circulation variability on sea ice cover in the Arctic Ocean, it has been suggested that anomalies of sea ice cover could potentially affect the atmosphere. The Atlantic sector might have greater impact on the atmospheric circulation, e.g., the Barents Sea revealed in a coupled atmosphere–ocean model[4], and the Greenland-to-Labrador seas shown in data[33] and investigated in a box model[34]. The low sea ice anomalies provide heat flux to the atmosphere over the Barents–Kara Sea, and then the perturbations propagate eastwards and intensify the high pressure in Siberia, such that even eastern Asia experiences cold winters[35-37]. This important aspect was not tackled in the present study, but we should challenge it by developing an atmospheric model and coupling it with the present ice–ocean model.

Acknowledgments The financial support by the Japanese Ministry of Education, Culture, Sport, Science, and Technology was fundamental to this work. Appreciation is acknowledged regarding fruitful discussions with Dr. J Overland, Dr. S Prinsenberg, Dr. J Wang, Dr. G Panteleev, Dr. J Zhang, Dr. K Mizobata, and Dr. X Zhang on the physical responses to climate variability, and also to Dr. M Kawai-Yamamoto, Dr. Y Watanabe, and Dr. S Tanaka on basic behaviors of biogeochemical tracers. Our gratitude is also extended to Mr. A Yamada for the solid analyses of various data sets, and to Mr. T Ikeda for editing the text with regard to the use of English.

References

1 Walsh J E, Overland J E, Croisman P Y, et al. Climate model projections for the Arctic//Arctic Monitoring and Assessment Programme(AMAP). Snow, Water, Ice and Permafrost in the Arctic (SWIPA): Climate Change and the Cryosphere. Oslo, Norway, 2011: 538.

2 Stroeve J, Holland M M, Meier W, et al. Arctic sea ice decline: Faster than forecast. Geophysical Research Letters, 2007: 34, L09501, doi:10.1029/2007GL029703.

3 Wang M, Overland J E. A sea ice free summer Arctic within 30 years: An update from CMIP5 models. Geophysical Research Letters , 2012, 39, L18501, doi:10.1029/2012GL052868.

4 Koenigk T, Mikolajewicz U, Jungclaus J H, et al. Sea ice in the Barents Sea: seasonal to interannual variability and climate feedbacks in a global coupled model. Climate Dynamics, 2009, 32: 1119-1138, doi:10.1007/s00382-008-0450-2.

5 Overland J E, Wang J, Walsh J E, et al. Climate model projections for the Arctic, Snow, Water, Ice and Permafrost in the Arctic (SWIPA): Climate Change and the Cryosphere, Oslo, Arctic Monitoring and Assessment Programme (AMAP), 2011.

6 Ikeda M. Sea-ice cover anomalies in the Arctic Basin associated with atmospheric variability from multi-decadal trends to intermittent quasi-biennial oscillations. Polar Research, 2012, 31, 18690, doi:10.3402/polar.v31i0.18690.

7 Thompson D W J, Wallace J M. The Arctic oscillation signature in the wintertime geopotential height and temperature fields. Geophysical Research Letters, 1998, 25: 1297-1300.

8 Polyakov I V, JohnsonM A. Arctic decadal and interdecadal variability. Geophysical Research Letters, 2000, 27: 4097-4100.

9 Rigor I G, Wallace J M, Colony R L. Response of sea ice to Arctic Oscillation. Journal of Climate, 2002, 15: 2648-2663.

10 Morison J, Steele M, Kikuchi T, et al. Relaxation of central Arctic Ocean hydrography to pre-1990s climatology. Geophysical Research Letters, 2006, 33, L17604, doi:10.1029/2006GL026826.

11 Zhang J, Lindsay R, Steele M, et al. What drove the dramatic retreat of arctic sea ice during summer 2007? Geophysical Research Letters , 2008, 35, L11505, doi:10.1029/2008GL034005.

12 Newton R, Schlosser P, Martinson D G, et al. Freshwater distribution in the Arctic Ocean: Simulation with a high-resolution model and model-data comparison. Journal of Geophysical Research, 2008, 113, C05024, doi:10.1029/2007JC004111.

13 Maslowski W, Kenney J C, Higgins M, et al. The future of Arctic sea ice. Annual Review of Earth and Planetary Sciences, 2012, 40: 625-654, doi:10.1146/annurev-earth-042711-105345.

14 Aagaard K, Carmack E C. The role of sea ice and other fresh water in the Arctic circulation. Journal of Geophysical Research, 1989, 94: 14485-14498.

15 Ikeda M. Wind effects on buoyancy-driven general circulation in a closed basin using a two-level model. Journal of Physical Oceanography, 1987, 17: 1707-1723.

16 Ikeda M, Colony R, Yamaguchi H, et al. Decadal variability in the Arctic Ocean shown in hydrochemical data. Geophysical Research

Letters, 2005, 32, L21605, doi:10.1029/2005GL023908.
17 Falkner K K, Steele M, Woodgate R A, et al. Dissolved oxygen extrema in the Arctic Ocean halocline from the North Pole to the Lincoln Sea. Deep-Sea Research, 2005, 52: 1138-1154.
18 Hydrochemical Atlas of the Arctic Ocean. St. Petersburg, State Research Center of the Russian Federation-the Arctic and Antarctic Research Institute of the Russian Federal Service for Hydrometeorology and Environmental Monitoring, and Fairbanks, International Arctic Research Center, University of Alaska, 2001.
19 Wilson C, Wallace D W R. Using the nutrient ratio NO/PO as a tracer of continental shelf waters in the central Arctic Ocean. Journal of Geophysical Research, 1990, 95: 22193-22208.
20 Ikeda M, Colony R, Yamaguchi H, et al. Decadal variability shown by the Arctic Ocean Hydrochemical Data and reproduced by an ice-ocean model. Journal of Ocean University of China, 2005, 4(4): 343-348.
21 Bryan K. A numerical method for the study of the circulation of the world ocean. Journal of Computational Physics, 1969, 4: 347-376.
22 Sasai Y, Ikeda M, Tanaka N. Air-sea CO2 flux during the mixed layer development in the northern North Pacific. Journal of Geophysical Research, 2000, 105: 3465-3481.
23 Hibler W D. A dynamic thermodynamic sea ice model. Journal of Physical Oceanography, 1979, 9: 815-846.
24 Hiraike Y, Ikeda M. Descending surface water at the Antarctic marginal ice zone and its contribution to the Intermediate Water using an ice-ocean model. Journal of Oceanography, 2009, 65: 587-603.
25 Ikeda M. Salt and heat balances in the Labrador Sea using a box model. Atmosphere-Ocean, 1987, 25: 197-223.
26 Maslowski W, Lipscomb W H. High resolution simulations of Arctic sea ice, 1979-1993. Polar Research, 2003, 22: 67-74.
27 Rothrock I G, Zhang J M. Arctic Ocean sea ice volume: What explains its recent depletion? Journal of Geophysical Research, 2005, 110, C01002, doi:10.1029/2004JC002282.
28 Aksenov Y, BaconS, Coward A C, et al. The North Atlantic inflow to the Arctic Ocean: high-resolution model study. Journal of Marine Systems, 2010, 79: 1-22.
29 Mysak L A, Venegas S A. Decadal climate oscillations in the Arctic: a new feedback loop for atmosphere-ice-ocean interactions. Geophysical Research Letters, 1998, 25: 3607-3610.
30 Jones E P, Anderson L G. On the origin of the chemical properties of the Arctic Ocean halocline. Journal of Geophysical Research, 1986, 91: 10759-10767.
31 Timmermans M L, Winsor P, Whitehead J A. Deep-water flow over the Lomonosov Ridge in the Arctic Ocean. Journal of Physical Oceanography, 2005, 35: 1489-1493.
32 Wu B, Overland J E, D'Arrigo R. Anomalous Arctic surface wind patterns and their impacts on September sea ice minima and trend. Tellus A, 2012, 64: 18590, http://dx.doi.org/10.3402/tellusa.v64i0.18590.
33 Strong C, Magnusdottir G, Stern H. Observed feedback between winter sea ice and the North Atlantic Oscillation. Journal of Climate, 2009, 22: 6021-6032, doi:10.1175/2009JCLI3100.1.
34 Ou H W. A box model of the Arctic natural variability. Climate Dynamics, 2013, 40: 1687-1706, doi:10.1007/s00382-012-1453-6.
35 Honda M, Inoue J, Yamane S. Influence of low Arctic sea-ice minima on anomalously cold Eurasian winters. Geophysical Research Letters, 2009, 36: L08707, doi:10.1029/2008GL037079.
36 Inoue J, Hori M, Takaya K. The role of Barents Sea ice in the wintertime cyclone track and emergence of a warm-Arctic cold-Siberian anomaly. Journal of Climate, 2012, 25: 2561-2568, doi: http://dx.doi.org/10.1175/JCLI-D-11-00449.1.
37 Vihma T. Effects of Arctic sea ice decline on weather and climate: a review. Surveys in Geophysics, 2014, 35: 1175–1214, doi: 10.1007/s10712-014-9284-0.